Published in final edited form as:

Structure. 2015 August 4; 23(8): 1482–1491. doi:10.1016/j.str.2015.06.013.

Structural basis for ceramide recognition and hydrolysis by human Neutral Ceramidase

Michael V. Airola[a,d], **William J. Allen**[b], **Michael J. Pulkoski-Gross**[c], **Lina M. Obeid**[a,d,e], **Robert C. Rizzo**[b], and **Yusuf A. Hannun**[a,d,1]

[a]Department of Medicine, Stony Brook University, Stony Brook, NY 11794

[b]Department of Applied Mathematics and Statistics, Stony Brook University, Stony Brook, NY 11794

[c]Department of Pharmacological Sciences, Stony Brook University, Stony Brook, NY 11794

[d]Stony Brook Cancer Center, Stony Brook, NY 11794

[e]Northport Veterans Affairs Medical Center, Northport, NY 11768

Summary

Neutral ceramidase (nCDase) catalyzes conversion of the apoptosis-associated lipid ceramide to sphingosine, the precursor for the proliferative factor sphingosine-1-phosphate. As an enzyme regulating the balance of ceramide and sphingosine-1-phosphate, nCDase is emerging as a therapeutic target for cancer. Here we present the 2.6 Å crystal structure of human nCDase in complex with phosphate that reveals a striking, 20 Å deep, hydrophobic active site pocket stabilized by a eukaryotic-specific subdomain not present in bacterial ceramidases. Utilizing flexible ligand docking, we predict a likely binding mode for ceramide that superimposes closely with the crystallographically observed transition state analog phosphate. Our results suggest nCDase uses a new catalytic strategy for Zn^{2+}-dependent amidases, and generates ceramide specificity by sterically excluding sphingolipids with bulky headgroups and specifically recognizing the small hydroxyl headgroup of ceramide. Together, this provides a foundation to aid drug development and establishes common themes for how proteins recognize the bioactive lipid ceramide.

Graphical Abstract

[1]To whom correspondence may be addressed: Yusuf A. Hannun, Department of Medicine, Stony Brook University, and the Stony Brook Cancer Center, Stony Brook, NY 11794, USA, Tel.: (631) 444-8067; yusuf.hannun@stonybrookmedicine.edu.

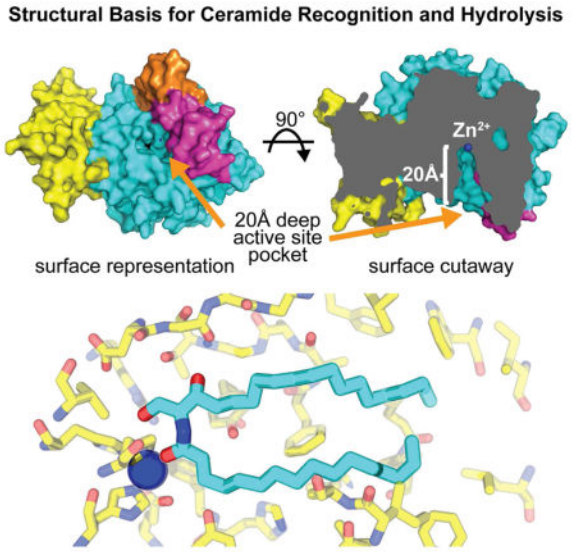

Keywords

Sphingolipids; Ceramidase; Crystallography; Ceramide; Docking

Introduction

Sphingolipids are a family of membrane lipids that play important roles in transducing cellular signaling processes (Hannun and Obeid, 2008). They can have a wide range of functional effects including promoting migration, cell proliferation, senescence, and apoptosis (Hannun and Obeid, 2008; Morad and Cabot, 2012; Ogretmen and Hannun, 2004; Spiegel and Milstien, 2003). Ceramide, sphingosine (Sph), and sphingosine-1-phosphate (S1P) are three of the most extensively-studied bioactive sphingolipid species (Futerman and Hannun, 2004; Hannun and Obeid, 2008). Ceramide lies at the center of sphingolipid metabolism and serves as a central hub for interconversion between sphingolipids (Airola and Hannun, 2013). Several enzymes control the levels and turnover of ceramide, and many of these ceramide-metabolizing enzymes have been proposed as candidate therapeutic targets in various conditions (Canals et al., 2011; García-Barros et al., 2013; Saied and Arenz, 2013). Moreover, their combined substrate specificities define the ceramide-centric metabolism of sphingolipids (Gault et al., 2010; Hannun and Obeid, 2002). However, the mechanisms by which these enzymes generate their specificity are unclear due to a lack of structural information.

Ceramidases (CDases) are lipid amidases that catalyze the hydrolysis of the amide bond of ceramide to form Sph and a fatty acid (Fig. 1A) (Mao and Obeid, 2008). CDases occupy a key role in sphingolipid metabolism by converting the apoptosis-associated lipid ceramide to Sph, a precursor for the proliferative factor S1P (Futerman and Hannun, 2004; Mao and Obeid, 2008). Three families of CDases (acid, neutral, and alkaline) have been identified that are distinguished by their pH optima, subcellular localization, primary structure, mechanism, and function (Mao and Obeid, 2008).

Neutral ceramidase (nCDase) is a single-pass transmembrane glycoprotein (El Bawab et al., 2000; Tani et al., 2000) that is highly expressed in the intestinal system and localizes to the brush border of intestinal and colonic epithelial cells (Kono et al., 2006). NCDase knockout mice are viable, but display altered intestinal sphingolipid levels and increased levels of ceramide in stool samples (Kono et al., 2006). The expression and activity of nCDase has been linked to cell-cycle arrest and growth regulation (Franzen et al., 2001; Osawa et al., 2005; Wu et al., 2009), which has established nCDase as an attractive target for pharmacological interventions (Canals et al., 2011; Saied and Arenz, 2013). An alternative form of nCDase with an altered N-terminus localizes to mitochondria (El Bawab et al., 2000) and has been implicated in the pathogenesis of traumatic brain injury (Novgorodov et al., 2014).

Human nCDase is a novel enzyme that defines a unique family of evolutionarily conserved CDases, which display little sequence homology to other proteins including acid and alkaline CDases (Mao and Obeid, 2008). NCDase displays strict substrate specificity for the endogenous stereoisomer of ceramide (El Bawab et al., 2002; Usta et al., 2001). Sphingolipids with modifications to the 1-hydroxyl headgroup of ceramide do not act as substrates. Thus, nCDase specifically hydrolyzes the amide bond of ceramide and not ceramide-1-phosphate, sphingomyelin, or glycosphingolipids (Fig. S1)

Bacterial nCDases from *P. aeruginosa* and *M. tuberculosis* have been cloned and implicated as exotoxins in these pathogens (Okino et al., 1999; Okino and Ito, 2007). Structural characterization of the bacterial nCDase (bCDase) from *P. aeruginosa* revealed a shallow active site cleft for ceramide hydrolysis (Inoue et al., 2009). Bacterial CDase was proposed to follow a similar catalytic mechanism to Zn^{2+}-dependent carboxypeptidase. However, this mechanism did not account for the unique tetra-coordinated Zn^{2+} ion and involved only one of the four strictly conserved active site residues. Furthermore, while bCDase shares some overall sequence identity with human nCDase (37%), the amino-acid sequence and length of key regions that form the active site differ, which suggests human nCDase may contain a unique active site pocket. This led us to structurally characterize human nCDase to gain insights into the molecular mechanism of this emerging therapeutic target.

Herein, we draw on structural, computational, and biochemical data to show that human nCDase is indeed a novel lipid amidase that contains a deep hydrophobic active site pocket for ceramide binding and hydrolysis. Based on active site interactions with the crystallographically observed transition state analog phosphate and flexible ligand docking of ceramide, we suggest nCDase employs a unique catalytic mechanism that involves stabilizing the transition state oxyanion through protein sidechain interactions and not by direct Zn-coordination. This differs in comparison to the proposed mechanisms of other Zn-dependent amidases, including bCDase (Finnin et al., 1999; Hernick and Fierke, 2005). Furthermore, our results shed light on how nCDase generates its strict substrate specificity towards ceramide. We propose nCDase uses the deep hydrophobic pocket that ends abruptly at the catalytic Zn^{2+} ion to (i) sterically exclude sphingolipids with larger headgroups and (ii) facilitate specific recognition of the small hydroxyl headgroup of ceramide. This represents the first structural characterization of a eukaryotic ceramide-metabolizing enzyme and a new molecular perspective into the function of this diverse set of proteins.

Results

Purification of active, glycosylated human nCDase

An extracellular region of human nCDase (residues 99–780, lacking the flexible O-glycosylated mucin box) was overexpressed in Sf9 cells as a secreted protein, purified by Ni-column and size-exclusion chromatography, and crystallized (Fig. S2). The purified protein was active towards the fluorescent substrate NBD-C12-Ceramide (Tani et al., 1999) with a K_m of 33 μM and a turnover number (k_{cat}) of 62 min^{-1} at 28°C (Fig. 1B). N-glycosylation of nCDase was confirmed by PNGaseF treatment (Fig. S2C).

Overall architecture

We determined the crystal structure of the N-glycosylated extracellular region of human nCDase in complex with phosphate at 2.6 Å resolution (Table 1). Two protein molecules were contained within the asymmetric unit that superimposed with an RMSD of 0.24 Å. The structure consists of a catalytic domain (residues 99–626), a short linker (627–641), and an immunoglobulin (IG)-like domain (642–780) (Fig. 2). Electron density was observed for all residues except the loop regions between amino acids 637–641, 686–687, and 758–761. The IG-like and catalytic domains are bridged by a Ca^{2+} ion that is coordinated by protein backbone interactions and the sidechain of Thr717. The base of the catalytic domain is formed by a novel three-β sheet triangle (Fig. S2) that represents a unique protein fold with a Dali search identifying bCDase as the only similar protein in the Protein Data Bank. A number of loops and secondary structural elements sit atop the β-triangle core to form the active site. Electron density for N-linked glycans was observed at Asn151, Asn217, Asn308, and Asn440 in the catalytic domain and Asn730 in the IG-like domain (Fig. 2B). Solvent-exposed disulfide bonds were present in the catalytic domain between Cys362-Cys376, Cys370-Cys384, and Cys448-Cys498, which indicates a likely explanation for the sensitivity of nCDase activity to reducing agents (Fig. 2B) (El Bawab et al., 1999; Galadari et al., 2006).

A deep, hydrophobic active site pocket

The active site of human nCDase is composed of a narrow, 20 Å deep, hydrophobic pocket with a Zn^{2+} ion at the base (Fig. 2C). The entrance to the hydrophobic active site pocket is unobstructed and solvent-accessible (Fig. 2C), and appears flexible with the highest B-factors observed in these regions of the protein. Hydrophobic residues line the pocket from top to bottom (Fig. 2D, 3E). One side of the active site cavity of human nCDase is formed by the η2-α8 helices, which have a divergent amino-acid sequence (Fig. 2G) and are repositioned in comparison to bCDase (Fig. 2B vs. 2E, and Fig. S3F–G). A 30-residue insertion, not present in bCDase, forms a novel, small disulfide-containing domain that interacts with the η2-α8 helices to stabilize their position (Fig. 2). An additional stabilizing factor is the third-disulfide bridge in nCDase, which ties together the beginning and end of the n2-a8 helix element and is conserved between human nCDase and bCDase (Fig. 2B, Fig. S4). Overall, the lipid-like contouring of the active site suggests that either no major rearrangements are necessary to accommodate ceramide, or that the Zn-bound phosphate is inducing an active conformation. To initially validate the hydrophobic pocket as the site of

ceramide hydrolysis, we introduced positively charged arginine residues at positions Gly124, Ala211, and Gly465 and determined their effects on nCDase activity (Fig. 4E).

Active site architecture and interactions with the transition state analog phosphate

A cluster of polar residues lies at the base of pocket that coordinates Zn^{2+} and interacts with bound phosphate (Fig. 3A). Canonical Zn-dependent amidases have three sidechains that coordinate to the proximal side of Zn^{2+}, and are typically Glu, Asp, or His residues, with the remaining two Zn-coordination sites occupied by water molecules (Hernick and Fierke, 2005). In comparison, human nCDase is unique in that four protein sidechains coordinate the Zn^{2+} and phosphate occupies the fifth Zn-coordination site. His194, His303, and Glu540 occupy the canonical, proximal Zn-coordinating positions, while Tyr579 coordinates to the opposite, distal face of the Zn^{2+} below phosphate (Fig. 3B).

Phosphate displays a tetrahedral coordination geometry, which serves as a mimic for the tetrahedral transition state of ceramide hydrolysis by nCDase. Analysis of residues in close proximity to phosphate helps to predict the likely interactions with ceramide during catalysis and provide insight into how nCDase stabilizes the tetrahedral transition state of hydrolysis. Phosphate interacts with three sidechains in the active site. His196 is located above the Zn^{2+} and coordinates to two phosphate oxygen atoms. Tyr579 and Tyr591, which are respectively below and behind phosphate, coordinate to the same phosphate oxygen atom. The positively charged guanidinium group of Arg257 is located in the active site and forms a hydrogen bond with Tyr579. Together, this suggests that His196, Arg257, Tyr579, and Tyr591 may all play critical roles in catalysis and stabilizing the transition state of ceramide hydrolysis. Of note, Ser354, previously identified as important for catalysis (Galadari et al., 2006), is located at the base of the pocket, 10 Å removed from the Zn^{2+} ion, and stabilizes the position of Arg257 through a hydrogen-bonding network (Fig. 4D).

Flexible ligand docking identifies a consensus pose for ceramide binding

To understand the molecular basis for substrate binding and hydrolysis, we computationally docked ceramide into the hydrophobic active site pocket of nCDase. A rigorous, flexible ligand docking protocol (Table S1) was employed to impartially dock ceramide (105 atoms, 34 rotatable bonds, and 2 chiral centers) into each of the two nCDase protein molecules (chains A and B) in the asymmetric unit. Approximately 400 unique ceramide binding poses were generated within each protein chain. Visual inspection of the top 50 most energetically favorable ceramide poses revealed a consensus pose that represented both (i) the single most favorable pose and (ii) ~50% of the top 50 poses to both chain A and B (Fig. 3C). In this consensus pose, the defining polar regions of ceramide superimposed with an RMSD of <1.0 Å and displayed heterogeneity only after carbon-11, near the exit of the hydrophobic pocket, where the lipid tails became solvent exposed (Fig. 3F). This model suggests nCDase must extract ceramide from the membrane for hydrolysis and may explain the preference for longer-chain length ceramides (Mao and Obeid, 2008). In addition, this explains how the bulky, hydrophilic NBD moiety of the commonly used substrate NBD-C12-ceramide is accommodated within the active site pocket of nCDase, as it is predicted to lie just outside the narrowest region of the hydrophobic pocket (Fig. S1). The highly reproducible computational predictions are credited to the well-defined active site pocket of nCDase that

appears finely tuned to accommodate the ceramide lipid (Fig. 3E–G). Superposition with the crystallographic phosphate found that the amide bond of ceramide was in a near identical position (Fig. 3D). This suggested that the predicted consensus pose might represent the ceramide binding mode during hydrolysis.

Catalytic mechanism and validation

Based on the interactions with phosphate and the predicted binding pose of ceramide, we propose a general acid-base catalysis (GABC) mechanism for amide bond hydrolysis by nCDase (Fig. 4A). In this mechanism, the Zn^{2+} ion functions to activate a water molecule for nucleophilic attack of the amide carbon. His196 serves as a general base for proton extraction from water and subsequently, a general acid to shuttle this proton to the nitrogen of ceramide during amide bond cleavage. In the crystal structure, His196 is the only sidechain within hydrogen-bonding distance to two oxygen atoms of phosphate (Fig. 3A), which in our model correspond to the position of the nucleophilic water and nitrogen atom in the amide bond of ceramide, and importantly, the proposed role is consistent with the neutral pH optima of nCDase. Tyr579 and Tyr591, each containing hydroxyl groups that form hydrogen bonds with the phosphate oxygen atom that faces away from Zn^{2+} (Fig. 3A), are predicted to polarize the carbonyl group and stabilize the carbonyl oxyanion formed after nucleophilic attack (Fig. 4A). Consistent with this mechanism, the mutations H196A, Y579F, and Y591F, as well as mutation of the three proximal Zn-coordinating residues, all abolished nCDase activity (Fig. 4E). Additional substitutions of H196 and Y579 designed to mimic the proposed functions also completely eliminated enzyme activity (Fig. S5), which is consistent with the strict sequence conservation of the active site core.

One caveat to our proposed mechanism is that the carbonyl oxygen atom in the predicted ceramide consensus pose occupies the position of the nucleophilic water molecule. Thus, the amide bond would need to rotate away from the Zn^{2+} to accommodate a water molecule and hydrogen bond with Tyr579 and Tyr591. To confirm this possibility, we re-docked ceramide into the active site with a water molecule placed in the same position as the Zn-coordinating oxygen atom of phosphate. Of the ~1,000 generated ceramide-binding poses, three distinct consensus conformations were identified that distributed approximately evenly among the top 150 most energetically favorable poses. While two of these poses were in positions that would not support hydrolysis, one of the new consensus poses was similar to the original consensus ceramide pose (Fig. S6), but with the amide bond flipped approximately 180° into a position available for hydrolysis (Fig. 4B). This suggested the proposed binding mode of ceramide in our catalytic mechanism is both energetically favorable and physically possible. As a final validation of this mechanism, we docked the transition state analog of ceramide (Fig. 4A, bottom right panel) with the amide carbonyl replaced with a tetrahedral carbon center containing an oxyanion and a hydroxyl group. This generated a ceramide consensus pose (Fig. S6) that superimposed with phosphate and made identical interactions with the sidechains of His196, Tyr579, and Tyr591 (Fig. 4C). Overall, our proposed mechanism identifies key roles for all the conserved residues in the active site and allowed us to predict how nCDase specifically recognizes ceramide and discriminates against other sphingolipids.

Molecular determinants of ceramide specificity and sphingolipid discrimination

A fundamental question in sphingolipid metabolism is how ceramide-metabolizing enzymes generate specificity for ceramide over other sphingolipid species. This specificity helps direct the ceramide-centric metabolism of sphingolipids that requires more complex sphingolipids to first be converted to ceramide in order for the amide bond to be hydrolyzed. For example, this prohibits the direct conversion of ceramide-1-phosphate (C1P), which has a phosphate at the 1-hydroxyl headgroup of ceramide, to sphingosine-1-phosphate.

We used our model to analyze the molecular interactions that contribute to ceramide recognition and sphingolipid discrimination in nCDase. In our model, the terminal 1-hydroxyl-headgroup of ceramide hydrogen bonds with the guanidinium group of Arg257, located at the base of the hydrophobic pocket, adjacent to the Zn^{2+} ion (Fig. 4D). This suggests Arg257 is essential for distinguishing ceramide from other sphingolipids. Consistent with this prediction, the mutation R257A completely eliminated nCDase activity (Fig. 4E). However, we note that the interaction between Arg257 and Tyr579 also appears critical and may contribute to the total loss of activity. We also attempted to alter the substrate specificity of nCDase by mutating Arg257 to various residues. However, all mutations completely eliminated nCDase activity towards ceramide (Fig. S5A), including the most conservative substitution R257K; and none of these mutations gained the ability to hydrolyze C1P (Fig. S5B).

The specific recognition of the ceramide headgroup by Arg257 indicates that steric hindrance precludes activity towards lipids with bulkier headgroups including C1P and 1-O-methyl ceramide (El Bawab et al., 2002; Galadari et al., 2006; Usta et al., 2001). Steric hindrance also provides a simple explanation for the lack of amidase activity towards sphingomyelin and glycolipids, which respectively contain even larger phosphocholine and sugar headgroups that cannot be accommodated within the well-defined active site of nCDase.

The critical position of Arg257 in the active site is stabilized by a series of hydrogen bonds between surrounding residues (Fig. 4D). These include direct hydrogen bonding interactions with the sidechains of Asp462 and Glu592. Asp462 makes an additional contact with Ser354. The hydrogen-bond network between Ser354-Asp462-Arg257 provides a rationale for the previous observation that the S354A mutation inactivates nCDase (Galadari et al., 2006).

An additional substrate-protein interaction was observed between the sidechain of Thr460 and the 3-hydroxyl group of ceramide (Fig. 4D). The mutation T460A significantly reduced, but did not eliminate nCDase activity (Fig. 4E). Previous studies found that nCDase could not hydrolyze ceramide with a methylated 3-hydroxyl position (El Bawab et al., 2002; Usta et al., 2001). The predicted hydrogen-bonding interaction with Thr460 is consistent with this finding and helps support the validity of our model.

The catalytic and IG-like domains are structurally and functionally linked

Human nCDase contains a C-terminal IG-like domain of unknown function that is conserved in the bacterial CDase exotoxins. The IG-like and catalytic domains are bridged by a Ca^{2+}

ion that is coordinated by the sidechain of Thr717, four carbonyl groups from the protein backbone, and a water molecule (Fig. 5A). To ascertain the role of the IG-like domain, we deleted the entire region (ΔIG) and mutated the sole Ca-coordinating sidechain of Thr717 in full-length nCDase. ΔIG completely lacked nCDase activity, while the T717A point mutation exhibited significantly decreased activity (Fig. 5B). Structural analysis finds that the Ca^{2+} ion and active site are physically linked by a series of β-sheet type interactions (Fig. 5C). We suggest that the IG-like domain and Ca^{2+} binding helps to stabilize the tertiary structure of nCDase and therefore contributes to catalytic activity, which is consistent with the conservation of the IG-like domain in bacterial CDases. We speculate that the IG-like domain of human nCDase may have additional roles in membrane recognition or protein-protein interactions that will require further investigation.

Discussion

Despite intense research over the past two decades, the structural basis underlying the ceramide-metabolizing activity of nCDase and related enzymes has remained elusive. This new structural information is the first view of how these lipid-metabolizing enzymes generate specificity and provides evidence that nCDase utilizes a unique mechanism for ceramide hydrolysis. As nCDase is an emerging therapeutic target, this may also aid in drug development.

Model for ceramide hydrolysis by nCDase

Human nCDase is highly expressed in the intestinal system and brain where ceramide is solubilized in bile acid micelles and membranes. The deep hydrophobic pocket of human nCDase differentiates it from its bacterial exotoxin counterparts and presents a model that human nCDase must at least partially extract ceramide, depending on the length of the acyl chain (Fig. 6). The highly O-glycosylated mucin box may serve as a flexible tether that enables nCDase to hydrolyze this bioactive lipid in these two different physiological forms (Fig. 6).

Mechanistic comparison with other Zn-dependent amidases

In light of our findings, we propose nCDase utilizes a unique catalytic strategy in comparison to other Zn-dependent amidases (Hernick and Fierke, 2005). The key difference lies in the occupation of the fourth Zn-coordination site by the hydroxyl group of Tyr579, which prevents direct coordination and polarization of the amide carbonyl group of ceramide by Zn^{2+}. In nCDase, we propose polarization of the amide carbonyl and stabilization of the transition state oxyanion occurs through interactions with the protein sidechains of Tyr579 and Tyr591, which both interact with the analogous phosphate-oxygen seen in the nCDase-phosphate complex. To our knowledge, all other mononuclear Zn-dependent amidases are proposed to directly coordinate both the hydroxyl group and oxyanion of the transition state to Zn^{2+} during catalysis (Hernick and Fierke, 2005). These include the enzymes carboxypeptidase, thermolysin, Class I and II HDACs, MMPs, and LpxC, which, with the exception of HDACs, all utilize an acidic residue as a general base for GABC (Hernick and Fierke, 2005). HDACs are the closest mechanistic example to nCDase, as they use His residues for GABC, and a Tyr residue, along with Zn-coordination, to stabilize the transition

state (Finnin et al., 1999). We did consider the opposite possibility where nCDase uses the Zn^{2+} ion to polarize the amide carbonyl bond and the Tyrosine residues to activate the water molecule for nucleophilic attack; however, this mechanism would require a more complicated proton-shuttling mechanism from Tyr579 to His196 and thus seems less favorable. In addition, our modeling of ceramide and the observed interactions with phosphate also strongly favor our proposed mechanism. We suspect the unique mechanism of nCDase may derive from the interaction of Tyr579 with both the positively charged Zn^{2+} ion and Arg257 sidechain. These interactions may induce a partial positive charge on the hydroxyl group of Tyr579 and explain how nCDase polarizes the amide carbonyl bond and stabilizes the negatively charged oxyanion during catalysis.

The unique mechanism of human nCDase is likely conserved by bCDase given the conservation of key catalytic residues (Fig. S4) and the ability to superimpose the docked ceramide molecule from the human structure into the shallow active site cleft of bCDase (Fig. S6). The proposed carboxypeptidase-type mechanism for bCDase is limited by the weakly observed electron density and high B-factors of residues that form the active site pocket (Fig. S3D) and the co-crystallized but non-hydrolyzed substrate C2-ceramide (Fig. 7). Our new structural information from human nCDase in complex with the transition state analog phosphate provides the necessary new insight to redefine the catalytic mechanism of this novel lipid amidase. Importantly, unlike the mechanism proposed for bCDase, our proposed mechanism identifies clear roles for all the conserved catalytic residues surrounding the tetra-coordinated Zn^{2+} ion.

Structural insight into the divergent functions of human and bacterial nCDase

Although human and bacterial nCDase catalyze the same reaction, their sites for binding ceramide differ drastically due to inherent differences in the proteins themselves, which reflects their divergent functions. As mentioned above, human nCDase functions in the turnover of ceramide within cell membranes and bile acid micelles. Consequently, the human structure contains a narrow active site pocket that contributes to the high degree of specificity. In contrast, bacterial nCDase from *P. aeruginosa* functions as an exotoxin that rapidly hydrolyzes ceramide within cell membranes. As such, the active site pocket appears to have evolved into an open, shallow cleft with a high degree of conformational flexibility to enable rapid ceramide turnover. This conformational flexibility is clearly visualized by the weak electron density for the η2-α8 helix region in the bCDase crystal structure and also indicated by the associated high temperature factors (Fig. S3). In addition, the co-crystallized C2-ceramide molecules are also not well ordered and display quite striking conformational flexibility (Fig. 7), which could indicate problems with the associated structure or reflect mobility, disorder, or low occupancy of the C2-ceramide molecules.

General strategies for ceramide recognition

The metabolism of sphingolipids is organized around ceramide as a central hub for lipid interconversion and is dictated by the strict substrate specificities of the three subtypes of CDases and the six mammalian ceramide synthases (Gault et al., 2010). This work establishes two related strategies that nCDase uses to generate specificity towards ceramide: (i) specific recognition of the 1-hydroxyl-headgroup of ceramide and (ii) discrimination of

larger headgroups through steric hindrance. Interestingly, ceramide recognition by ceramide transfer protein (CERT) has been demonstrated to utilize the same two strategies for distinguishing ceramide from other lipids (Fig. S7) (Kudo et al., 2008). This suggests these mechanisms may be a conserved feature of ceramide-binding proteins and it will be important in the future to compare the approaches utilized by other currently uncharacterized ceramide-interacting proteins.

Developing nCDase as a therapeutic target

NCDase is emerging as a therapeutic target for colon cancer and traumatic brain injury. This is based on studies using a mouse model of traumatic brain injury (Novgorodov et al., 2014), findings that nCDase is a target for the action of chemotherapeutics (Wu et al., 2009), and unpublished results from our group (Hannun lab) identifying nCDase as an important factor in the carcinogenesis of colon cancer. This work provides key insights that may aid in developing nCDase as a drug target: (i) it identifies nCDase as a Zn-dependent amidase and suggests hydroxamate-containing compounds may be candidates for nCDase inhibition (Onishi et al., 1996), (ii) the well-defined active site pocket and successful computational predictions suggest *in silico* docking and virtual screening may be a viable strategy to identify lead compounds, and (iii) the establishment of a crystallization system will facilitate co-crystal structures with lead compounds identified using the methods above, or with the recently generated high-throughput screening strategies now available for human nCDase, for structure activity refinement (Bedia et al., 2010; Bhabak et al., 2013; Saied and Arenz, 2013).

Methods

Protein expression, purification, and structure determination

The extracellular region (residues 99–780) of human nCDase with a C-ter 6x-His-tag and an N-ter insect secretory signal was expressed in Sf9 cells using baculovirus. Secreted nCDase protein was purified from the media using a 5 mL HisTrap excel column (GE Healthcare) and size-exclusion chromatography on a Hi-Load 26–60 Superdex 200 column equilibrated in 100 mM NaCl, 10 mM HEPES, pH 7.0. Pooled nCDase fractions were concentrated to 3 mg/mL and flash frozen. Crystals were obtained by hanging-drop vapor diffusion at 16°C by mixing equal volumes nCDase protein and reservoir solution over 0.2 M Li_2SO_4, 10% PEG 1K, and 0.1 M citrate-phosphate buffer at pH 4.6. X-ray diffraction data was collected at the BNL NSLS X29A beamline on an ADSC Quantum 315 CCD. Data were processed using XDS (Kabsch, 2010) and Scala as implemented in the autoPROC pipeline (Vonrhein et al., 2011). Molecular replacement with *P. aeruginosa* bCDase (PDB ID 2ZWS) was carried out in PHENIX (Adams et al., 2010). Three rounds of positional and thermal factor refinement in COOT (Emsley and Cowtan, 2004) and PHENIX (Adams et al., 2010) resulted in the final structure. During the first refinement the insertion domain was manually built, after which electron density for the α8 helix appeared. After the second refinement, electron density for the α2 helix appeared. Data collection and refinement statistics are provided in Table 1. Coordinates and structure factors for human nCDase have been deposited in the Protein Data Bank under accession code 4WGK.

Docking calculations

The ligand C16-ceramide was prepared in MOE (Chemical Computing Group, 2009) and assigned semi-empirical AM1-BCC charges (Jakalian et al., 2000; Jakalian et al., 2002) using the Amber tool antechamber (Case et al., 2005; Wang et al., 2006). Chains A and B of nCDase were aligned in a common reference frame using the matchmaker tool of UCSF Chimera (Pettersen et al., 2004) (αC RMSD=0.41 Å). The metal ions Zn^{2+} and Ca^{2+} were retained, and all other solvent particles were removed. Hydrogen atoms were added with MOE, and energy minimized using the Amber tool sander for 1000 cycles with a 1000.0 kcal mol^{-1} $Å^{-2}$ restraint on the heavy atoms. Following standard preparation protocols (Brozell et al., 2012; Mukherjee et al., 2010), a surface of each receptor chain was generated using DMS (2003), surface spheres were generated within the proposed binding site (21 spheres in chain A, 17 spheres in chain B) using sphgen (DesJarlais et al., 1988), then separate boxes with 20 Å margins in all directions were generated around the sphere sets. The program GRID (Meng et al., 1992) was used to generate an 0.3 Å resolution energy grid within the box boundaries using 6–9 Lennard-Jones coefficients to model attractive and repulsive van der Waals interactions, respectively, and a distance-dependent dielectric of ε=4.0r in the Coulomb potential to model electrostatic interactions. All docking calculations were performed using DOCK 6 (Allen et al., 2015) and standard flexible ligand protocols (Brozell et al., 2012; Mukherjee et al., 2010), with the exception that the RMSD restraint minimizer was activated with a restraint of 5.0 kcal mol^{-1} $Å^{-2}$ on ligand heavy atoms, and the minimum anchor size oriented to the binding site was 3 heavy atoms. Key docking run parameters are provided in Table S1.

Biochemical assays

Ceramidase activity using the fluorescent substrate NBD-C12-Ceramide (Avanti Polar Lipids) was conducted as described previously, with minor modifications (Galadari et al., 2006). Full-length nCDase constructs were expressed in *S. cerevisiae* cells with the galactose inducible pYES3 vector. Amino acid mutations were verified by DNA sequencing. Protein expression was confirmed by western blotting, which found all mutants behaved similar to wild type nCDase with no significant changes in yield and no apparent changes in glycosylation status. NCDase activity was quantitated by peak area comparison of the fluorescent NBD-fatty acid product with standards using an isocratic HPLC method in 100% methanol on a C18:1 Luna column.

Supplementary Material

Refer to Web version on PubMed Central for supplementary material.

Acknowledgments

We thank the beamline staff at BNL NSLS X29A beamline, Profs. Miguel Garcia-Diaz and Markus Seeliger (Stony Brook University) for access to crystallization facilities, Kip Guja for assistance with glycan refinement, and Ben Newcomb for assistance with virus amplification. This work was funded in part by the SBU Office of the Vice President for Research, NIH grants R01CA172517 (Y.A.H.), F32GM100679 (M.V.A.), R01GM097741 (L.M.O.), T32GM007518 (M.P-G.), and a MERIT Award BX000156 from the U.S. Dept. of Veterans Affairs (L.M.O.). This research utilized resources at the NY Center for Computational Sciences at SBU/BNL and the SBU Center for Structural Biology.

References

Adams PD, Afonine PV, Bunkóczi G, Chen VB, Davis IW, Echols N, Headd JJ, Hung LW, Kapral GJ, Grosse-Kunstleve RW. PHENIX: a comprehensive Python-based system for macromolecular structure solution. Acta Crystallographica Section D: Biological Crystallography. 2010; 66:213–221. [PubMed: 20124702]

Airola MV, Hannun YA. Sphingolipid Metabolism and Neutral Sphingomyelinases. Sphingolipids: Basic Science and Drug Development (Springer). 2013:57–76.

Allen WJ, Balius TE, Mukherjee S, Brozell SR, Moustakas DT, Lang PT, Case DA, Kuntz ID, Rizzo RC. DOCK 6: Impact of new features and current docking performance. Journal of Computational Chemistry. 2015; 36:1132–1156. [PubMed: 25914306]

Bedia C, Camacho L, Abad JL, Fabriàs G, Levade T. A simple fluorogenic method for determination of acid ceramidase activity and diagnosis of Farber disease. Journal of lipid research. 2010; 51:3542–3547. [PubMed: 20871013]

Bhabak KP, Hauser A, Redmer S, Banhart S, Heuer D, Arenz C. Development of a Novel FRET Probe for the Real - Time Determination of Ceramidase Activity. Chem Bio Chem. 2013; 14:1049–1052.

Brozell SR, Mukherjee S, Balius TE, Roe DR, Case DA, Rizzo RC. Evaluation of DOCK 6 as a pose generation and database enrichment tool. Journal of computer-aided molecular design. 2012; 26:749–773. [PubMed: 22569593]

Canals D, Perry DM, Jenkins RW, Hannun YA. Drug targeting of sphingolipid metabolism: sphingomyelinases and ceramidases. British journal of pharmacology. 2011; 163:694–712. [PubMed: 21615386]

Case DA, Cheatham TE, Darden T, Gohlke H, Luo R, Merz KM, Onufriev A, Simmerling C, Wang B, Woods RJ. The Amber biomolecular simulation programs. Journal of Computational Chemistry. 2005; 26:1668–1688. [PubMed: 16200636]

Chemical Computing Group. MOE. 2009.

DesJarlais RL, Sheridan RP, Seibel GL, Dixon JS, Kuntz ID, Venkataraghavan R. Using shape complementarity as an initial screen in designing ligands for a receptor binding site of known three-dimensional structure. Journal of medicinal chemistry. 1988; 31:722–729. [PubMed: 3127588]

El Bawab S, Bielawska A, Hannun YA. Purification and characterization of a membrane-bound nonlysosomal ceramidase from rat brain. Journal of Biological Chemistry. 1999; 274:27948–27955. [PubMed: 10488143]

El Bawab S, Roddy P, Qian T, Bielawska A, Lemasters JJ, Hannun YA. Molecular cloning and characterization of a human mitochondrial ceramidase. Journal of Biological Chemistry. 2000; 275:21508–21513. [PubMed: 10781606]

El Bawab S, Usta J, Roddy P, Szulc ZM, Bielawska A, Hannun YA. Substrate specificity of rat brain ceramidase. Journal of lipid research. 2002; 43:141–148. [PubMed: 11792733]

Emsley P, Cowtan K. Coot: model-building tools for molecular graphics. Acta Crystallographica Section D: Biological Crystallography. 2004; 60:2126–2132. [PubMed: 15572765]

Finnin MS, Donigian JR, Cohen A, Richon VM, Rifkind RA, Marks PA, Breslow R, Pavletich NP. Structures of a histone deacetylase homologue bound to the TSA and SAHA inhibitors. Nature. 1999; 401:188–193. [PubMed: 10490031]

Franzen R, Pautz A, Bräutigam L, Geisslinger G, Pfeilschifter J, Huwiler A. Interleukin-1β induces chronic activation and de novo synthesis of neutral ceramidase in renal mesangial cells. Journal of Biological Chemistry. 2001; 276:35382–35389. [PubMed: 11457826]

Futerman AH, Hannun YA. The complex life of simple sphingolipids. EMBO reports. 2004; 5:777–782. [PubMed: 15289826]

Galadari S, Wu Bxax, Mao C, Roddy P, El Bawab S, Hannun Yxaa. Identification of a novel amidase motif in neutral ceramidase. Biochem J. 2006; 393:687–695. [PubMed: 16229686]

García-Barros M, Coant N, Truman J-P, Snider AJ, Hannun YA. Sphingolipids in colon cancer. Biochimica et Biophysica Acta (BBA)-Molecular and Cell Biology of Lipids. 2013

Gault CR, Obeid LM, Hannun YA. An overview of sphingolipid metabolism: from synthesis to breakdown. Sphingolipids as signaling and regulatory molecules (Springer). 2010:1–23.

Hannun YA, Obeid LM. The ceramide-centric universe of lipid-mediated cell regulation: stress encounters of the lipid kind. Journal of Biological Chemistry. 2002; 277:25847–25850. [PubMed: 12011103]

Hannun YA, Obeid LM. Principles of bioactive lipid signalling: lessons from sphingolipids. Nature reviews Molecular cell biology. 2008; 9:139–150. [PubMed: 18216770]

Hernick M, Fierke CA. Zinc hydrolases: the mechanisms of zinc-dependent deacetylases. Archives of biochemistry and biophysics. 2005; 433:71–84. [PubMed: 15581567]

Inoue T, Okino N, Kakuta Y, Hijikata A, Okano H, Goda HM, Tani M, Sueyoshi N, Kambayashi K, Matsumura H. Mechanistic insights into the hydrolysis and synthesis of ceramide by neutral ceramidase. Journal of Biological Chemistry. 2009; 284:9566–9577. [PubMed: 19088069]

Jakalian A, Bush BL, Jack DB, Bayly CI. Fast, efficient generation of high - quality atomic Charges. AM1 - BCC model: I. Method. Journal of Computational Chemistry. 2000; 21:132–146.

Jakalian A, Jack DB, Bayly CI. Fast, efficient generation of high - quality atomic charges. AM1 - BCC model: II. Parameterization and validation. Journal of Computational Chemistry. 2002; 23:1623–1641. [PubMed: 12395429]

Kabsch W. Xds. Acta Crystallographica Section D: Biological Crystallography. 2010; 66:125–132. [PubMed: 20124692]

Kono M, Dreier JL, Ellis JM, Allende ML, Kalkofen DN, Sanders KM, Bielawski J, Bielawska A, Hannun YA, Proia RL. Neutral ceramidase encoded by the Asah2 gene is essential for the intestinal degradation of sphingolipids. Journal of Biological Chemistry. 2006; 281:7324–7331. [PubMed: 16380386]

Kudo N, Kumagai K, Tomishige N, Yamaji T, Wakatsuki S, Nishijima M, Hanada K, Kato R. Structural basis for specific lipid recognition by CERT responsible for nonvesicular trafficking of ceramide. Proceedings of the National Academy of Sciences. 2008; 105:488–493.

Mao C, Obeid LM. Ceramidases: regulators of cellular responses mediated by ceramide, sphingosine, and sphingosine-1-phosphate. Biochimica et Biophysica Acta (BBA)-Molecular and Cell Biology of Lipids. 2008; 1781:424–434. [PubMed: 18619555]

Meng EC, Shoichet BK, Kuntz ID. Automated docking with grid - based energy evaluation. Journal of Computational Chemistry. 1992; 13:505–524.

Morad SA, Cabot MC. Ceramide-orchestrated signalling in cancer cells. Nature Reviews Cancer. 2012; 13:51–65. [PubMed: 23235911]

Mukherjee S, Balius TE, Rizzo RC. Docking validation resources: protein family and ligand flexibility experiments. Journal of chemical information and modeling. 2010; 50:1986–2000. [PubMed: 21033739]

Novgorodov SA, Riley CL, Yu J, Borg KT, Hannun YA, Proia RL, Kindy MS, Gudz TI. Essential roles of neutral ceramidase and sphingosine in mitochondrial dysfunction due to traumatic brain injury. Journal of Biological Chemistry. 2014; 289:13142–13154. [PubMed: 24659784]

Ogretmen B, Hannun YA. Biologically active sphingolipids in cancer pathogenesis and treatment. Nature Reviews Cancer. 2004; 4:604–616. [PubMed: 15286740]

Okino N, Ichinose S, Omori A, Imayama S, Nakamura T, Ito M. Molecular Cloning, Sequencing, and Expression of the Gene Encoding Alkaline Ceramidase from Pseudomonas aeruginosa CLONING OF A CERAMIDASE HOMOLOGUE FROM MYCOBACTERIUM TUBERCULOSIS. Journal of Biological Chemistry. 1999; 274:36616–36622. [PubMed: 10593963]

Okino N, Ito M. Ceramidase enhances phospholipase C-induced hemolysis by Pseudomonas aeruginosa. Journal of Biological Chemistry. 2007; 282:6021–6030. [PubMed: 17202150]

Onishi HR, Pelak BA, Gerckens LS, Silver LL, Kahan FM, Chen MH, Patchett AA, Galloway SM, Hyland SA, Anderson MS. Antibacterial agents that inhibit lipid A biosynthesis. Science. 1996; 274:980–982. [PubMed: 8875939]

Osawa Y, Uchinami H, Bielawski J, Schwabe RF, Hannun YA, Brenner DA. Roles for C16-ceramide and sphingosine 1-phosphate in regulating hepatocyte apoptosis in response to tumor necrosis factor-α. Journal of Biological Chemistry. 2005; 280:27879–27887. [PubMed: 15946935]

Pettersen EF, Goddard TD, Huang CC, Couch GS, Greenblatt DM, Meng EC, Ferrin TE. UCSF Chimera—a visualization system for exploratory research and analysis. Journal of Computational Chemistry. 2004; 25:1605–1612. [PubMed: 15264254]

Saied E, Arenz C. Small molecule inhibitors of ceramidases. Cellular physiology and biochemistry: international journal of experimental cellular physiology, biochemistry, and pharmacology. 2013; 34:197–212.

Spiegel S, Milstien S. Sphingosine-1-phosphate: an enigmatic signalling lipid. Nature reviews Molecular cell biology. 2003; 4:397–407. [PubMed: 12728273]

Tani M, Okino N, Mitsutake S, Ito M. Specific and sensitive assay for alkaline and neutral ceramidases involving C12-NBD-ceramide. Journal of biochemistry. 1999; 125:746–749. [PubMed: 10101288]

Tani M, Okino N, Mori K, Tanigawa T, Izu H, Ito M. Molecular Cloning of the Full-length cDNA Encoding Mouse Neutral Ceramidase A NOVEL BUT HIGHLY CONSERVED GENE FAMILY OF NEUTRAL/ALKALINE CERAMIDASES. Journal of Biological Chemistry. 2000; 275:11229–11234. [PubMed: 10753931]

UCSF Computer Graphics Laboratory. DMS. 2003.

Usta J, Bawab SE, Roddy P, Szulc ZM, Hannun YA, Bielawska A. Structural requirements of ceramide and sphingosine based inhibitors of mitochondrial ceramidase. Biochemistry. 2001; 40:9657–9668. [PubMed: 11583166]

Vonrhein C, Flensburg C, Keller P, Sharff A, Smart O, Paciorek W, Womack T, Bricogne G. Data processing and analysis with the autoPROC toolbox. Acta Crystallographica Section D: Biological Crystallography. 2011; 67:293–302. [PubMed: 21460447]

Wang J, Wang W, Kollman PA, Case DA. Automatic atom type and bond type perception in molecular mechanical calculations. Journal of molecular graphics and modelling. 2006; 25:247–260. [PubMed: 16458552]

Wu BX, Zeidan YH, Hannun YA. Downregulation of neutral ceramidase by gemcitabine: Implications for cell cycle regulation. Biochimica et Biophysica Acta (BBA)-Molecular and Cell Biology of Lipids. 2009; 1791:730–739. [PubMed: 19345744]

Highlights

- Reports the first structure for a eukaryotic ceramide metabolizing enzyme (nCDase)
- Reveals a deep hydrophobic pocket for binding the bioactive lipid ceramide
- Establishes how nCDase distinguishes ceramide from related lipids
- Identifies a new type of catalytic strategy for Zn^{2+}-dependent amidases

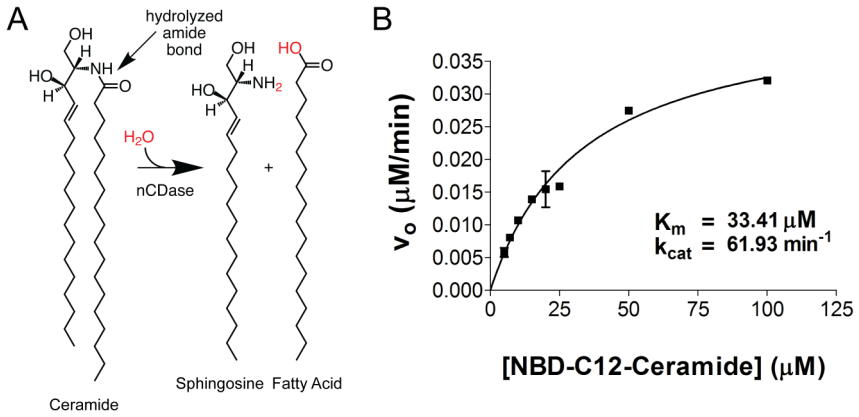

Figure 1. Characterization of purified human nCDase

(A) Neutral ceramidase hydrolyzes the amide bond of ceramide to generate sphingosine and free fatty acid. **(B)** Initial velocity (μM/min) vs. substrate concentration (μM) of purified human nCDase activity towards NBD-C12-Ceramide. K_m and k_{cat} values are indicated. Reactions were conducted with 5 ng purified nCDase at 28°C for multiple time points between 15 min – 2 hrs. (See also Figure S1)

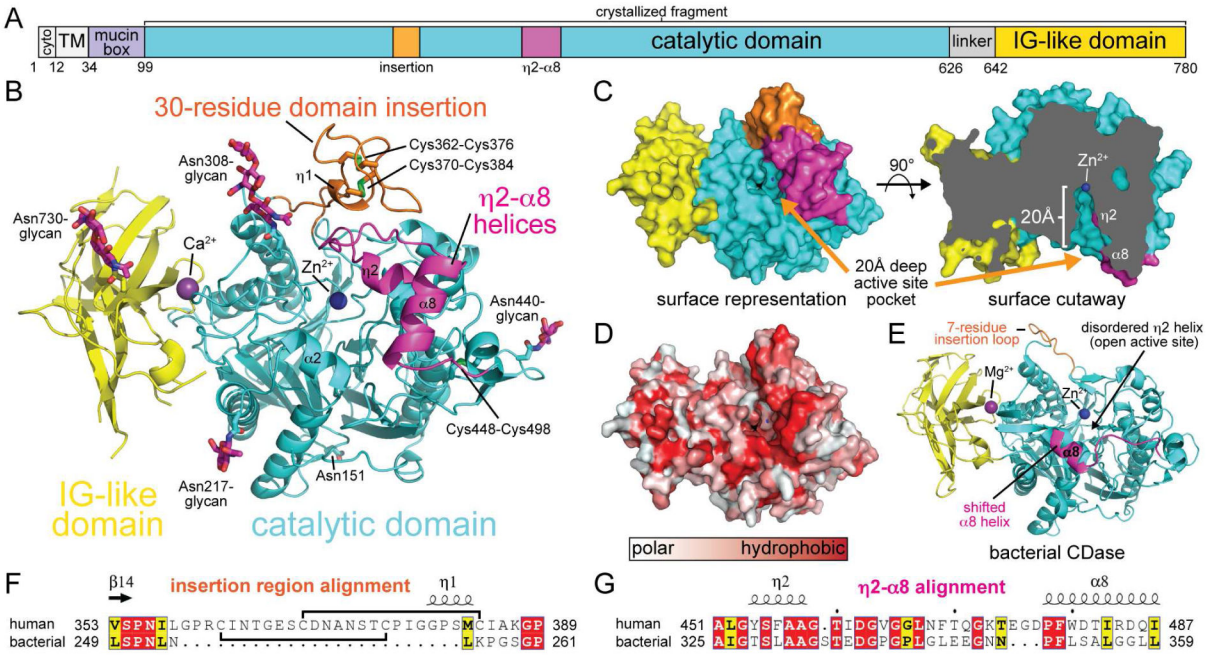

Figure 2. Crystal structure of human nCDase reveals a novel, 20 Å deep hydrophobic active site pocket

(A) Domain organization of human nCDase. **(B)** Crystal structure of the catalytic and IG-like domains of human nCDase (PDB ID 4WGK). Catalytic domain, cyan; IG-like domain, yellow; domain insertion, orange; η2-α8 helices, magenta. Asn-linked N-glycans are shown as magenta sticks. The Asn151-glycan was only observed in one nCDase molecule and is not shown. The bound Zn^{2+} and Ca^{2+} ions are shown as blue and violet spheres, respectively. Disulfide linkages are shown as sticks. **(C)** Surface representation and surface cutaway of human nCDase highlighting the 20 Å deep, active site pocket. **(D)** Hydrophobic surface representation of human nCDase. **(E)** B-factor representation of the human nCDase crystal structure. **(F)** Sequence alignment of the insertion region and **(G)** η2-α8 region from human nCDase and bacterial CDase highlighting the divergent sequences that form the deep hydrophobic pocket in human nCDase. Connecting lines indicates disulfide bonds. (See also Figure S2–S4)

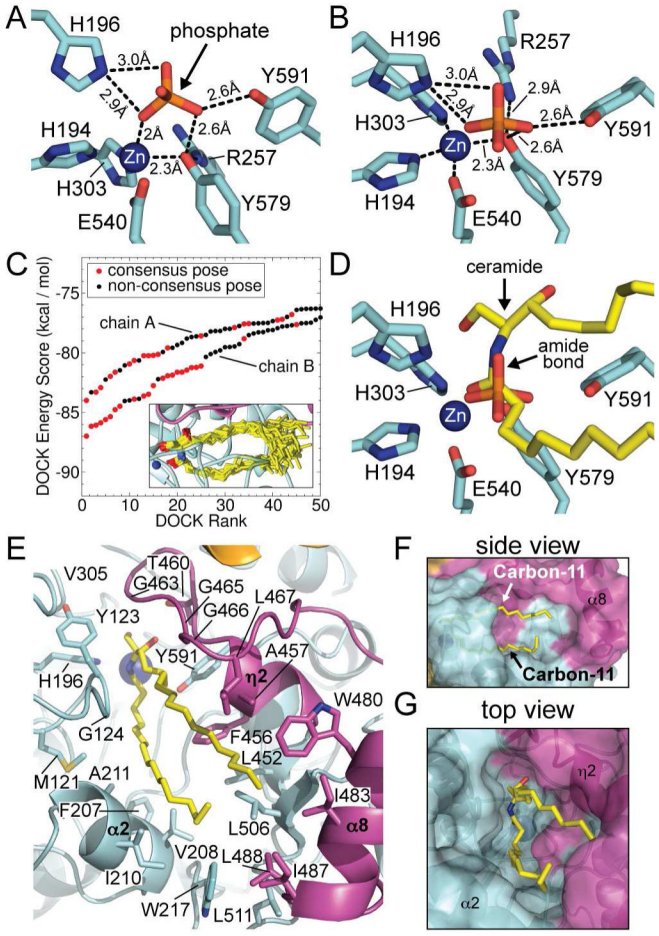

Figure 3. Active site interactions with phosphate and ceramide

(A) NCDase active site highlighting interactions with phosphate and the four Zn-coordinating sidechains from side and **(B)** top views. Phosphate, orange and red sticks. **(C)** Dock ranking by energy score of the top 50-ceramide binding poses. Consensus and non-consensus poses are shown as red and black circles, respectively. (inset) Overlay of ceramide consensus poses. **(D)** Active site interactions with overlay of phosphate and lowest energy ceramide consensus pose in same view as panel B. **(E)** Cartoon depiction of ceramide in the active site with surrounding hydrophobic side chains shown as sticks. **(F, G)** Surface representations of ceramide in the active site pocket from side and top views. (see also Figure S6)

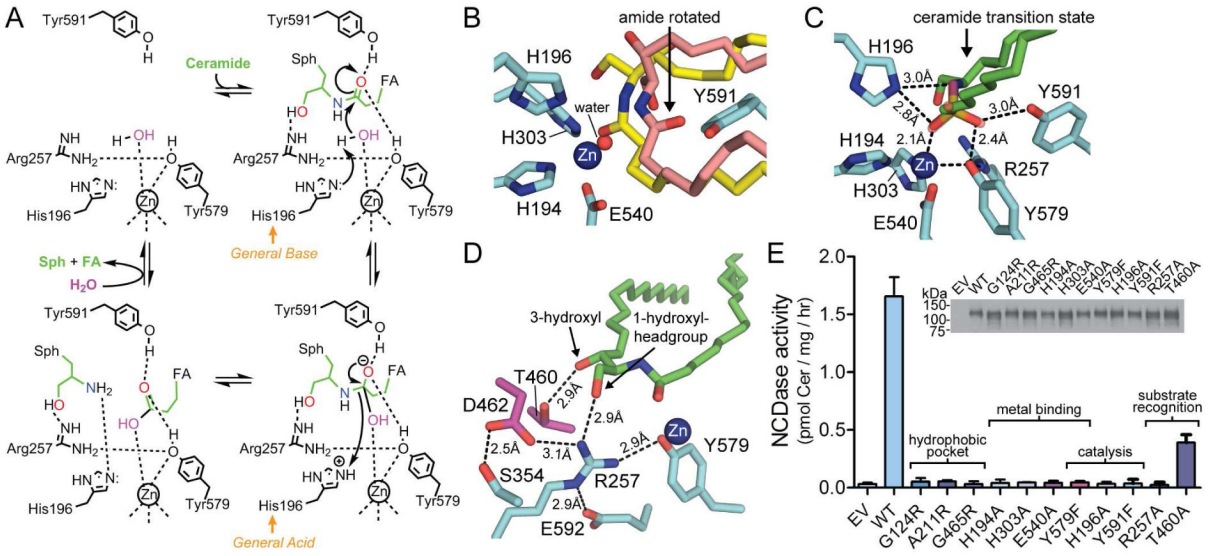

Figure 4. Catalytic mechanism and ceramide recognition

(A) Proposed catalytic mechanism. Bottom right panel, tetrahedral transition state. **(B)** Overlay of ceramide consensus poses with the amide bond rotated for hydrolysis, pink sticks. The water molecule present in the docking calculations is shown as a red sphere. **(C)** Side view of docked ceramide transition state highlighting identical active interactions as the crystallographic-observed transition state analog phosphate. **(D)** Substrate recognition of the hydroxyl headgroup of ceramide by R257. A network of hydrogen bonds involving the sidechains of S354, D462, and E592 stabilizes the position of R257. T460 interacts with the 3-hydroxyl of ceramide. Distances are between the lowest energy ceramide transition state pose. **(E)** Activity and expression of nCDase active site mutants. Data are shown as mean ± SD from three to six independent experiments. All mutants behaved similar to wild type nCDase with no significant changes in yield and no apparent changes in glycosylation status. (see also Figure S5 and S7)

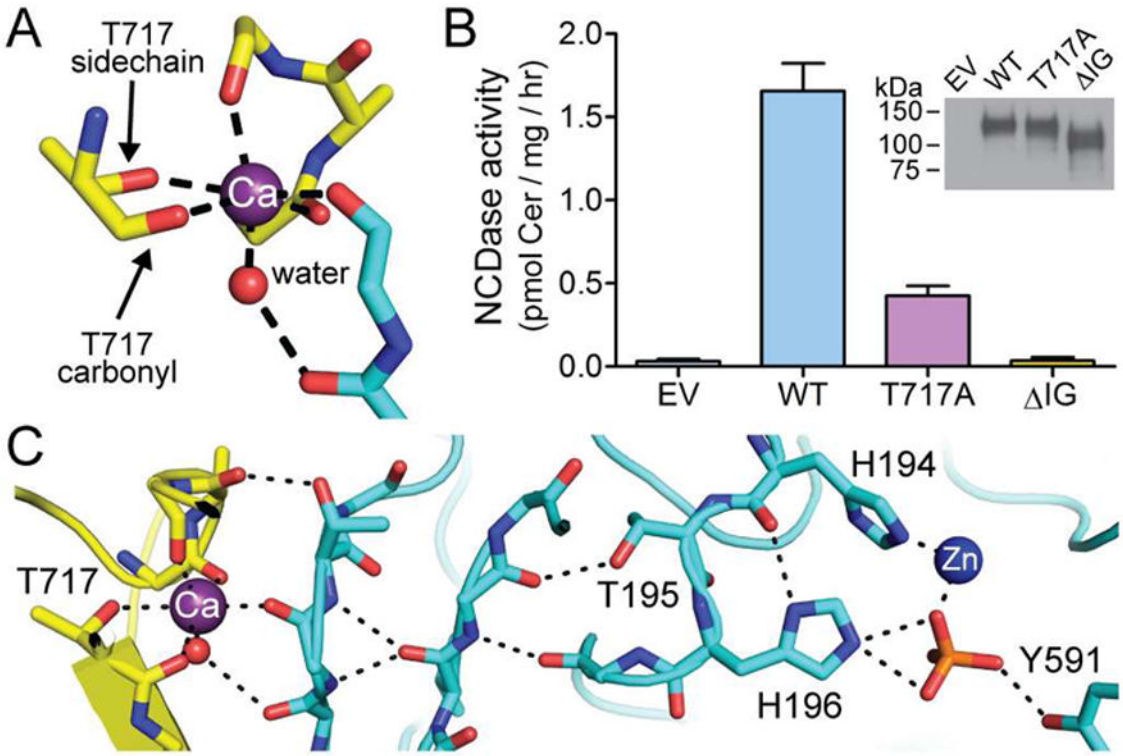

Figure 5. The catalytic and immunoglobulin-like domains are structurally and functionally linked

(A) Ca^{2+} is coordinated between the IG-like (yellow) and catalytic (cyan) domains by six oxygen atoms from the sidechain of Thr717, four carbonyl groups in the peptide backbone, and a water molecule. **(B)** Activity and expression of T717A and **Δ**IG nCDase mutants. Data are shown as mean ± SD from three to six independent experiments. **(C)** The active site loop containing the essential His194 and His196 residues are linked to the Ca^{2+} binding site through a series of β-sheet type interactions.

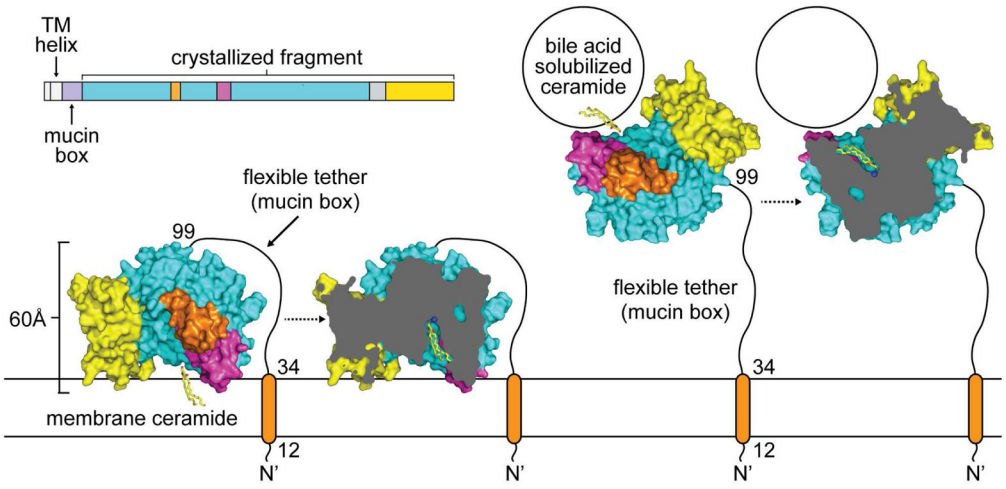

Figure 6. Model of ceramide hydrolysis by nCDase in membranes and bile-acid micelles

Schematic of ceramide hydrolysis by the membrane-tethered human nCDase involves extracting ceramide from membranes (left) or bile-acid micelles (right) into the deep hydrophobic pocket. The flexible tether would allow human nCDase to hydrolyze ceramide in these two different physiological forms.

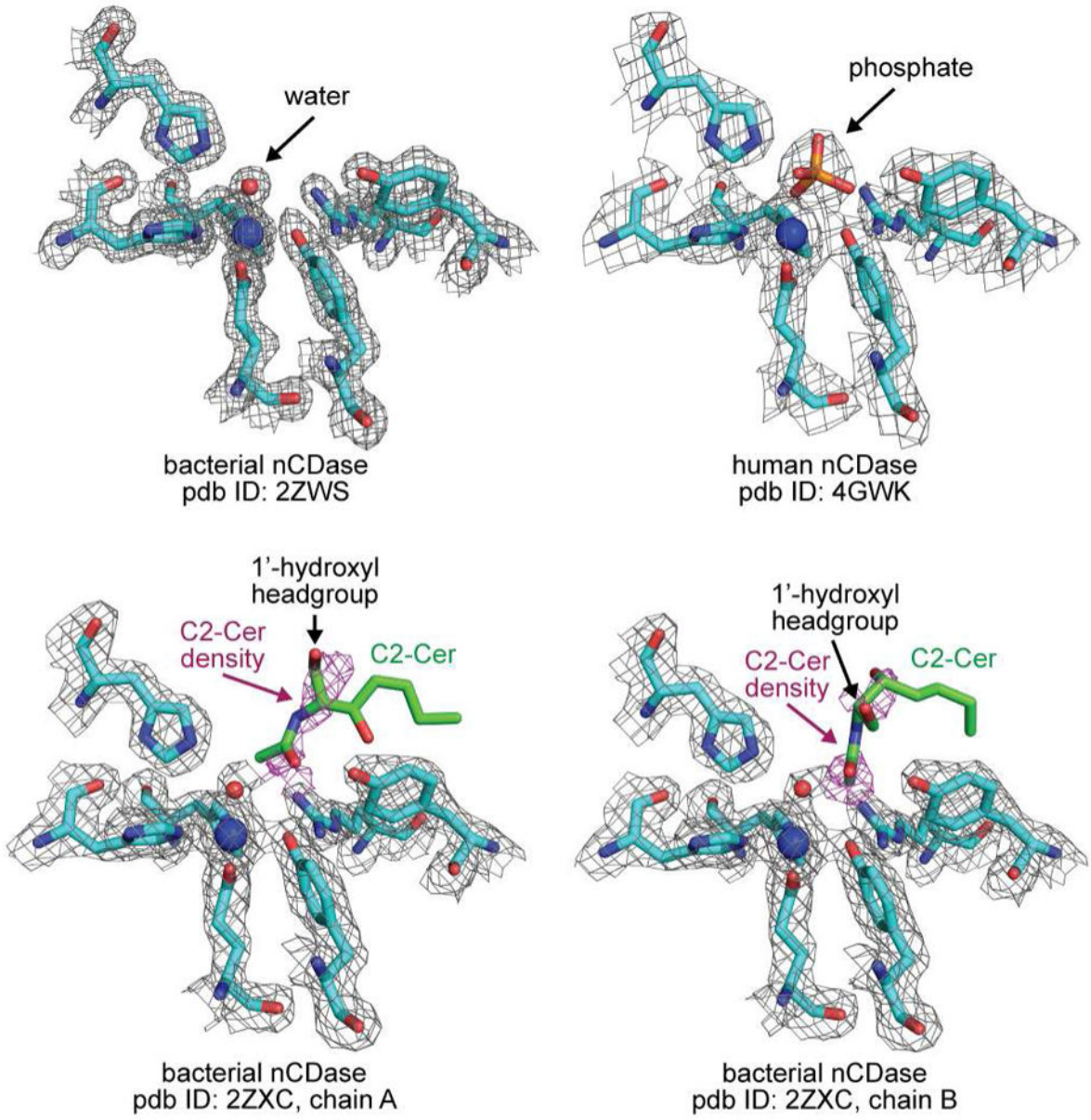

Figure 7. $2F_o$-F_c electron density maps of human and bacterial nCDase active sites

$2F_o$-F_c electron density maps of human and bacterial nCDase active sites contoured at 1.5 σ. The phosphate (human) and water (bacterial) molecules bound to Zn^{2+} fit well within the electron density maps. C2-Ceramide (C2-Cer) electron density (magenta) does not contour around the C2-Cer molecules (green), which occur in two differing binding modes with the amide bond in a non-hydrolysable position in both chains. This may indicate problems with the associated structure or reflect conformational flexibility from mobility, disorder, or low occupancy of the C2-ceramide molecules. Figures were generated by downloading the electron density maps in ccp4 format from the Protein Data Bank and visualized in PyMOL.

Table 1

Crystallographic data collection and refinement statistics

	Human nCDase (PDB ID 4WGK)
Data collection	
Wavelength, Å	0.987
Resolution range, Å	68.65–2.582 (2.674–2.582)
Space group	$P2_1$
Unit cell dimensions	
a, b, c, Å	73.48, 156.63, 80.33
α, β, γ, °	90, 108.04, 90
Total reflections	90770 (8225)
Unique reflections	49612 (4716)
Multiplicity	1.8 (1.7)
Completeness, %	91.63 (87.4)
R_{merge}	0.0805 (0.3726)
<I>/<σI>	7.42 (1.90)
Refinement	
R_{work}/R_{free}	17.8 (25.8)/22.3 (32.3)
No. atoms	11142
Protein	10408
Ligand/ion	240
Water	494
B-factors, $Å^2$	31.2
Protein	30.8
Ligand/ion	52.8
Water	29.3
RMS	
Bond lengths, Å	0.003
Bond angles, °	0.67
Ramachandran favored (%)	98
Ramachandran outliers (%)	0

Values in parentheses are for highest-resolution shell